Simulation of the expansion within a vacuum chamber of the plume of a Hall thruster with a centrally mounted cathode

A. Modesti[1], J. Zhou[1], F. Cichocki[2], A. Domínguez-Vázquez[1], E. Ahedo[1]

[1]Equipo de Propulsión Espacial y Plasmas, Universidad Carlos III de Madrid, Leganés, Spain,
[2]Istituto per la Scienza e Tecnologia dei Plasmi (ISTP), CNR, Bari, Italia,

Email: alberto.modesti@uc3m.es, jiewei.zhou@uc3m.es, filippo.cichocki@istp.cnr.it, adrian.dominguez@uc3m.es, eduardo.ahedo@uc3m.es

KEYWORDS:

EP2PLUS, hybrid PIC-fluid code, magnetized plume, staggered scheme, Hall Effect Thruster, ground facility, vacuum chamber simulations

ABSTRACT

The simulation of a Hall effect thruster and its plume interaction with the spacecraft and ground facilities is of great importance for the design and development phases. In the frame of H2020 ASPIRE project (Advanced Space Propulsion for Innovative Realization of Space Exploration), several studies are going to be conducted in order to assess the role of vacuum chamber back-pressure, chamber walls and electric circuit behavior. In the frame of the project PROMETEO and in order to model the involved physics, an in-house 3D hybrid PIC-fluid code, called EP2PLUS [1], has been upgraded. It features an equivalent electric circuit solver employing a simplified sheath model, several surface properties for plasma-object interaction, and a non-linear Poisson's equation solver to better characterize non-neutral plasma regions especially near the side and rear metallic walls of the thruster assembly. The magnetized electrons are treated as a polytropic fluid subject to both collisions and magnetic field effects, and the heavy species are simulated as macro-particles of a particle-in-cell model. The output of this demonstration study is a simplified but still self-consistent simulation of an HET plume expansion in a vacuum chamber scenario. An assessment of stray currents in the Direct Drive "grounded CRP" strategy [2] complements the results.

1 INTRODUCTION

1.1 Hall Effect Thrusters' plumes

Hall Effect thrusters (HET) are one of the most mature, robust and reliable technology in the electric propulsion field. In particular they can be operated with moderately low voltages and power levels, maintaining an adequate efficiency and a lifetime compatible with the more ambitious modern mission goals. [3]

HET plume characteristics are defined by the combined effects of the dynamics of charged particles, which compose the relatively rarefied plume itself, and the thruster magnetic field. The knowledge of the plasma plume evolution in the surrounding space is of fundamental importance at system design level, for new generation satellites, in order to integrate the propulsive subsystem with the other vehicle subsystems: indeed, compatibility problems are common in electro-magnetic propulsive equipments, and they are typically due to the electrically charged particle flow, which can interfere with telecommunication signals and generate erosion and insulation loss for critical satellite surfaces (e.g. solar panels, optical instruments and sensors etc.). To acquire and extend this knowledge, experiment and simulations play a fundamental role.

1.2 Numerical simulations of HET plumes

It is generally difficult to compare or extrapolate directly results from ground facility to the free space of the operational thruster conditions, mainly because a comprehensive simulation taking into account a realistic chamber geometry and electric circuit, the pumping system performance and the effect of the sputtering caused by the plume ions is extremely challenging to achieve. A particularly ambitious simulation goal is represented by the quantitative estimation of the vacuum chamber system (geometry and pumping system) effects on the overall ground operation, and not only in terms of the thruster performance from a merely propulsive point of view.

It is known [4] that the presence of the background pressure, mainly due to the non perfect pumping action, can be seen as an adverse condition for the heavy species leaving the thruster exit. These molecules, in ground facilities, are expected to move somewhat slowly out of the thruster increasing the residence time within the thruster acceleration region and the related collision probability. This in turn implies a slightly increased ionization and an extremely increased production of slow charge-exchange (CEX) ions. Moreover, the fact that the chamber has solid walls influences significantly the operations, and it is not trivial to take it into account in simulations, where different boundary conditions (for electric potential and current, or for electron temperature in electron fluid models) can be adopted.

Therefore, an analysis with a 3D code, which takes into account the actual chamber dimensions and also the plasma sheaths and non-neutral zones forming at the chamber and thruster case lateral and back surface, is something that could shed some light on ground facility effects. Furthermore, a 3D and in-scale pressure and density topology of the neutral background is certainly more representative than the usually assumed uniform background pressure due to lack of experimental information related to the actual pressure gradients within the chamber itself.

Numerical models for the magnetized plasma plume expansion under magnetic field effect are of different types. A first approach is that of the kinetic approaches, which can be split into methods solving a simplified Boltzmann's equation for the ion and electron distribution functions in a low dimensional space (typically 1D, [5]), and full particle-in-cell (PIC) models [6], featuring particle ions/electrons, collisions through Montecarlo approaches [7], and generally limited to 2D to reduce the computational cost. An alternative approach, which is computationally cheaper, is that of hybrid codes, in which electrons are modeled as a fluid, while neutrals and ions are followed as macro-particles of a PIC submodel featuring Montecarlo collisions.

The 3D code EP2PLUS [1] makes use of this hybrid approach, and has already been used in different plasma thruster scenarios, from S/C-debris-plasma interaction in an ion beam shepherd scenario [8] to a plasma plume expansion under the geomagnetic field [9], including also simulations of 3D Hall thruster near plumes [10] and ion grid optics [11]. The magnetized electron model of Refs. [9, 10] is particularly appropriate to simulate the plasma expansion under a complex HET magnetic topology. Such a model solves the coupled electric current continuity and electron momentum balance equations, retaining both the electron collisions term and the very relevant magnetic force term, $\boldsymbol{j}_{\mathrm{e}} \times \boldsymbol{B}$, where $\boldsymbol{j}_{\mathrm{e}}$ is the electron current density and $\boldsymbol{B}$ is the magnetic induction field. In addition, non-neutral regions can be treated with a non linear Poisson solver, while the self-consistent plasma object interaction [1] is made possible through an equivalent electric circuit featuring an integrated sheath model. This simulator complexity and self consistency make it the most suitable tool to analyze the complete behavior of a HET plume, not only in free space [10], but also inside a ground facility under experimental conditions, featuring different kind of objects and behaviors that have to be accounted for.

1.3 Thruster plume characterization in ground facility

The recent developments in high-power Hall thruster systems are enabling a wide set of mission scenarios, thanks to the optimal combination of performance and reliability. These technological advantages, coupled with the increasing power available on-board satellite platforms, are encouraging several spacecraft manufacturers to focus on the implementation of high-power Hall-effect Electric Propulsion Systems (EPS). Despite potential advantages, several factors have limited the possibility of reaching the qualified status for these systems, such as huge costs and availability of suitable test facilities. H2020 ASPIRE project aims at increasing to 6 the Technology Readiness Level (TRL) of the HT20k 20 kW Hall-effect EPS inherited from CHEOPS H2020 project. The project will cover many aspects, such as the development of alternative/supporting qualification strategies for enabling reduced-cost qualification.

Since HT20k's magnetic topology is not available for the large experimental facility employed, the demonstration study presented here was performed with a HT5k-type thruster (medium power), with a Sitael's IV4-type facility domain with a simplified objects setup. The experimentally investigated configurations are several (differing by the amount of surface covered by dielectric, or by the size of the thruster assembly rear metallic plate), so a default scenario is adopted where the thruster has the whole front surface covered by dielectric material, apart from the channel and cathode surfaces, while the side and back walls are metallic.

In experiments, the architecture presented as Direct Drive "grounded CRP" approach [2] is adopted. The numerical models aim to reproduce an equivalent effect of this approach, and to enrich this study with a stray current assessment in the chosen configuration, to further validate the model against the experimental trends and behaviors.

This numerical study can be considered a first demonstration of an in-house multi-model simulator. The objective of the latter is a self-consistent reproduction of the experimental behavior of this complex experimental architecture by means of an equivalent electric circuit model coupled with fluid and particle models (non-neutral effects, heavy particle collisions, plasma-object interaction). After this first demonstration study with simplified models and hypotheses, an upgrade of the latter is foreseen, and the comparison against experimental results will allow to gain more insight into the main physical mechanisms. In addition, this kind of validation enables the possibility to extend the study to scenarios and regimes outside the experimental ground capabilities, such as in free space. A numerical simulator with this level of completeness would be of great use for this technology development process.

This paper is structured as follows. Sec. 2 introduces the numerical models for the performed simulations, in terms of PIC (Sec.2.1) and magnetized electron fluid (Sec.2.2) models, as well as the electric circuit, sheath model, and non neutral solver responsible for the simulation of the self-consistent plasma-objects interaction (Sec. 2.3). Then Sec. 3 reports the numerical simulation results obtained with the two models, after adding details about magnetic field and collisions, simulation and other physical parameters (Sec. 3.1) and on the boundary conditions for both the PIC and electron fluid modules respectively in Sec. 3.2.1 and Sec. 3.2.2. Then, a preliminary study needed to design background conditions for the chamber and its loss surfaces is described in Sec.3.3, while Sec.3.4 presents the complete plasma simulation results, featuring all the described models. Sec.3.5 provides an assessment of the stray current collected by the thruster assembly in a Direct-Drive equivalent scenario. Finally, Sec. 4 outlines the main conclusions of the study.

2 3D MAGNETIZED PLUME MODEL

The EP2PLUS code (Extensible Parallel Plasma PLUme Simulator), is a three-dimensional hybrid PIC-fluid code, which was firstly presented at the 2016 Space Propulsion Conference [12] in a free-space plasma-spacecraft interaction scenario. For this specific study, it is relevant to summarize the magnetized electron fluid model employed in the simulations. Regarding the particle-in-cell model for ion and neutral species, its main features are summarized in Sec.2.1.

2.1 PIC model

In summary (refer to Ref. [1] for details), the ion and neutral distribution functions are discretized in the position-velocity phase-space with a given number of macro-particles. By weighting them to the nodes of a structured PIC mesh, bulk properties like their number density, fluid velocity and temperature can be obtained. For each time-step, the PIC performs the following operations:

1. Moving macro-particles according to Newton's law, under electrostatic and magnetostatic fields;
2. Injecting new macro-particles into the simulation from the boundaries (see Fig. 6 and Fig.7) and eliminating particles that leave the domain;
3. Performing collisions between macro-particles with both MCC and DSMC approaches (see Ref. [1]), and generating/eliminating macro-particles due to sink/source collisional events (e.g. due to ionization);
4. Weighting the macro-particles to the mesh nodes to obtain their bulk properties (used by the electron model).

The modeled collisions include charge-exchange (CEX) and ionization collisions, as further described in Sec.3.1.

2.2 Magnetized electron model

The electron fluid model is the same as the one described in Ref. [9], but with a different numerical discretization strategy [13] already described and successfully applied in Ref. [9]. The model here assumes a simplified polytropic and isotropic electron thermodynamics. These hypotheses allow to derive the generalized Ohm's law from the electron momentum balance equation as [9]:

$$\boldsymbol{j} = -\mathcal{K}\cdot(\sigma_\mathrm{e}\nabla\Phi + \boldsymbol{j}_\mathrm{c}) + \boldsymbol{j}_\mathrm{i}, \qquad \text{(Eq. 1)}$$

At steady state, the total electric current density $\boldsymbol{j} = \boldsymbol{j}_\mathrm{e} + \boldsymbol{j}_\mathrm{i}$ satisfies the continuity equation with no source terms:

$$\nabla\cdot\boldsymbol{j} = 0. \qquad \text{(Eq. 2)}$$

where $\sigma_\mathrm{e} = e^2 n_\mathrm{e}/(m_\mathrm{e}\nu_\mathrm{e})$ is the electron scalar conductivity, $\boldsymbol{j}_\mathrm{c}$ is an effective current density grouping collisional effects with heavy species [9], and $\mathcal{K}$ is the normalized conductivity tensor, defined as:

$$\mathcal{K} = \begin{bmatrix} 1 & \chi b_3 & -\chi b_2 \\ -\chi b_3 & 1 & \chi b_1 \\ \chi b_2 & -\chi b_1 & 1 \end{bmatrix}^{-1}, \qquad \text{(Eq. 3)}$$

where $\mathbf{1}_\mathrm{b} = [b_1, b_2, b_3]$ is the unit vector along the applied magnetic field, so that $\boldsymbol{B} = B\mathbf{1}_\mathrm{b}$.
A "residual thermalized potential" Φ has been introduced. The latter is defined so that $\nabla\Phi = \nabla\phi - \nabla h_\mathrm{e}/e$, being ϕ the electric potential and $\nabla h_\mathrm{e} = \nabla p_\mathrm{e}/n_\mathrm{e}$ the barotropic function gradient (which is an exact differential when polytropic electrons are considered [9]). The gradient of the thermalized potential Φ in Eq. 1 measures the correction to be applied to the Boltzmann's electric field due to the effects of both magnetic field and collisions on the electron fluid [9].
The effective current density is defined as $\boldsymbol{j}_\mathrm{c} = en_\mathrm{e}/\nu_\mathrm{e}\sum_{s=1}^{L}\nu_{\mathrm{e}s}\boldsymbol{u}_s$, where the summation extends over the L considered heavy species, and $\nu_\mathrm{e} = \sum_{s=1}^{L}\nu_{\mathrm{e}s} + \nu_\mathrm{an}$ is the total electron momentum

transfer collision frequency, which also includes an anomalous collision frequency $\nu_{\rm an}$. The models for $\nu_{\rm es}$ are described in Ref. [1] and include the effect of both ionization collisions, and elastic collisions with neutrals and ions. The anomalous collision frequency $\nu_{\rm an}$ follows a Bohm's like transport [14] and is computed as $\nu_{\rm an} = \alpha_{\rm an}\omega_{\rm ce}$, with $\omega_{ce} = eB/m_{\rm e}$ the electron gyro-frequency. Here, $\alpha_{\rm an} = 2.5\%$, which permits to limit the effective Hall parameter $\chi = \omega_{\rm ce}/\nu_{\rm e}$ to a maximum value of 40, thus improving the solver's convergence, although it has been verified that the physical solution is only dimly affected by the chosen value.
Assuming the same reference point for Φ, $h_{\rm e}$ and ϕ, we have

$$\phi = \Phi + h_{\rm e}/e, \qquad \text{(Eq. 4)}$$

hence, the electric potential can be retrieved from the knowledge of $h_{\rm e}(n_{\rm e})$ (known from the PIC) and of the unknown Φ. For an electron polytropic coefficient γ, the barotropic function depends only on the quasineutral plasma density $n_{\rm e}$ [15]:

$$h_{\rm e} = -\frac{\gamma T_{\rm e0}}{(\gamma-1)}\left[1-\left(\frac{n_{\rm e}}{n_{\rm e0}}\right)^{\gamma-1}\right], \qquad \text{(Eq. 5)}$$

with $n_{\rm e0}, T_{\rm e0}$ the quasineutral plasma density and electron temperature at the reference plasma point - chosen to be in the middle of the annular channel exit - for the polytropic law:

$$T_{\rm e} = T_{\rm e0}\left(\frac{n_{\rm e}}{n_{\rm e0}}\right)^{\gamma-1} \qquad \text{(Eq. 6)}$$

Note that at the polytropic reference point for electron temperature and density, the electric potential ϕ_0 is not zero.

The numerical approach for the discretization of Eqs. 2 and 1 is a 1^{st} order hybrid Finite Volume (FV) - Finite Differences (FD) scheme on a staggered mesh [13]. In particular, Eq. 2 is discretized with FV, while Eq. 1 with FD schemes. Fig. 1 shows a 2D representation of the unknowns locations, which are the electric current densities at cell face centers and the thermalized potentials at cell centers, including ghost cells at the boundaries.

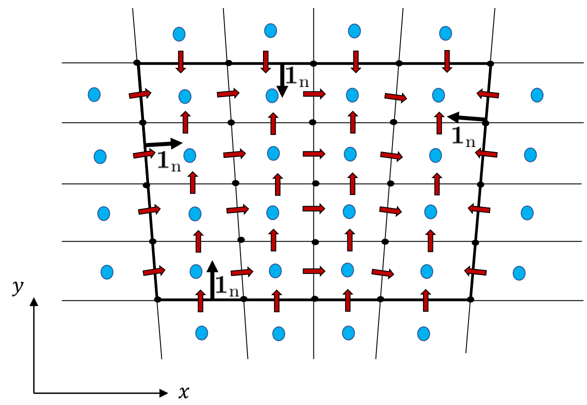

Figure 1: *Sketch of a 2D $x-y$ cross section of a slightly deformed staggered mesh, showing the locations of the unknowns. The solid bold black line represents the external boundary, black dots the mesh nodes, blue circles the cell centers at which Φ is solved for, and red arrows the normal components of $\boldsymbol{j}$, solved at cell faces centers. Taken from [16].*

This scheme is conservative due to the Finite Volume discretization of the continuity equation with a negligible global continuity error, so that there is no need for a very fine mesh as considered in Refs. [9, 10] and applied in [16], and the computational cost is significantly lower. In addition, FD schemes are centered everywhere (no need for forward/backward schemes at the boundaries), which leads to a lower discretization error. After the discretization on the staggered mesh, Ohm's law, Eq. 1, is substituted into the continuity equation, Eq. 2, leading to a system of equations in the unknown thermalized potential:

$$[M]\{\Phi\} = \{R\}. \qquad \text{(Eq. 7)}$$

with $[M]$ a square matrix with maximum rank obtained by imposing the Dirichlet condition on Φ at the cathode emission surface cell face centers, and $\{R\}$ a right hand side vector.

2.3 Ancillary models

Equivalent circuit solver, sheath models and non-neutral Poisson solver employed are described in [1]. Here their main features are summarized.

The sheath module is in charge of computing the boundary conditions for both the electric potential and the electric currents at the simulation boundaries (both material and external). This is done by assuming both a simplified sheath and an equivalent circuit models. First of all, the ion currents to the simulation objects are computed, from the knowledge of the ion particle fluxes to the material cell-faces (surface-weighted values). Then, the electron currents to the same simulation objects are computed with a simplified plasma sheath model.

The total electric current (sum of ion and electron current) is then used by the equivalent electric circuit, which updates the conductive object potentials.

After the equivalent circuit solution and continuity and momentum equation solution in quasi-neutral regime, the quasineutral solution for the electron density n_e^* is known, the simulation domain is dynamically split into quasineutral and non-neutral subdomains (according to a criterion base on a "non-neutrality" value assigned to each node), and the solution is updated in the non-neutral subdomain via the non-linear Poisson solver.
Once the electric potential has been computed and updated, the corresponding electric field (necessary to move ion macro-particles) is obtained.

3 NUMERICAL SIMULATIONS

3.1 Simulation settings

Heavy species (xenon neutral atoms, singly-charged ions and doubly charged ions) are distinguished into: background neutrals, injected neutrals, CEX neutrals from recombination, fast injected single ions, single ions from collision processes, fast injected doubly-charged ions, doubly-charged ions from collision processes.
Collisions between heavy species (ionization and CEX) are described in Tab.1.

Table 1: *Heavy species collisions. The additional electron as ionization output is taken into account in the electron fluid conservation equations.*

Collision	Input	Output
Ionization	Xe_{inj} + e	Xe^{+} + 2e
Ionization	Xe^{+} + e	Xe^{++} + 2e
CEX	Xe_{bg} + Xe^{+}_{fast}	Xe_{fast} + Xe^{+}_{slow}
CEX	Xe_{bg} + Xe^{++}_{fast}	Xe_{fast} + Xe^{++}_{slow}
CEX	Xe_{inj} + Xe^{+}_{fast}	Xe_{fast} + Xe^{+}_{slow}
CEX	Xe_{inj} + Xe^{++}_{fast}	Xe_{fast} + Xe^{++}_{slow}

In addition, background neutrals are imported from the pump study simulations of Sec. 3.3, and they are also generated by the diffuse neutrals reflection and the ions recombination at the walls. The initial background neutrals population corresponds to a steady state in a scenario featuring a total emitted thruster mass flow in the form of neutrals only (no ions). This is done to reduce the overall computational cost by decoupling the neutrals filling phase from that of the plasma ions, which require a lower time step (they move much faster). The consequence is that the real stationary conditions (in terms of neutrals background) with the thruster ignited are not reproduced faithfully, but only in an approximate fashion.

The magnetic field topology (Fig.3) is a complex magnetic shielding one retrieved from the solution of a magnetic circuit design for the virtual thruster considered (Fig. 2).

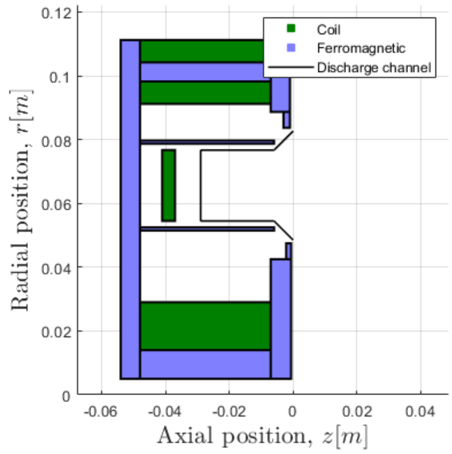

Figure 2: *Magnetic circuit schematics.*

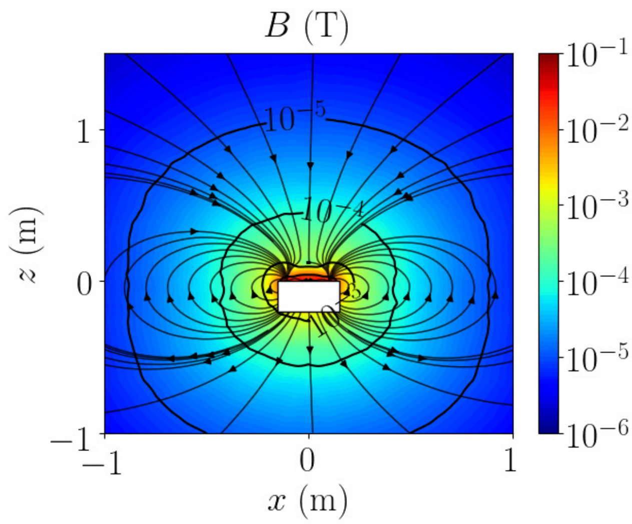

Figure 3: *Chamber magnetic topology generated from the magnetic circuit employed. Reference frame is rotated to appreciate the symmetry of the field.*

Other relevant physical and computational simulation parameters are summarized in Tab.2.

The injection profiles at the HET annular exit plane, and the prescribed normal electron current there, are obtained from full-thruster 2D simulations carried out with the code of Ref. [17], averaged in time as described in [10]. These are representative of the chosen nominal operation point of the thruster (15 A of discharge current, 300 V of discharge voltage, 14 mg/s of mass flow from the hannel, 1.05 mg/s of neutrals mass flow from the cathode). The reference point for the electron temperature (polytropic law) is located in the middle of the annular channel exit of the thruster.

Table 2: *Simulation parameters.*

Simulation parameters	Units	Values
Reference electron temperature (T_{e0})	eV	20.0
Electron polytropic cooling coefficient γ	n/a	1.35
PIC time-step	s	2.5$\cdot 10^{-7}$
Simulation duration	s	7.5$\cdot 10^{-4}$
Time-averaging steps for PIC sub-model	n/a	500
Anomalous transport coefficient α_{an}	-	2.5%

The main elements of the equivalent circuit model (see Fig4) are:

- the metallic chamber independent object which charges with respect to the plasma through an equivalent capacity (at steady state there will be a 0 net current flowing to the chamber walls);
- the thruster metallic case independent object, which is the equipotential reference for $\phi = 0$;
- the dielectric front surface of the thruster assembly, which receives no net electric current from the plasma;
- the cathode wall, which is kept at a fixed wall potential with respect to the thruster case, and from whose surface both neutrals and electrons are emitted. The potential at the cathode plasma is however different from the cathode object potential (as if a thin plasma sheath existed), and is obtained from the solution of the electron conservation equations.

The circuit configuration allows to compute the stray current $I_{stray} = I_{p,1}$, which at steady state is $I_{p,1} = I_{an} - I_{cat}$ being I_{an} the electric current exiting the thruster exit (equal to the anode current), and I_{cat} the elelctric current entering the cathode. Further description of the approach and the analysis is provided in Sec.3.5.

The employed mesh is a rectangular structured non-uniform one (the simulation domain is therefore a parallelepiped, even if the chamber is cylindrical). Domain dimensions are similar to Sitael's IV4 facility [3]. The domain boundaries consist in the chamber walls, including 4 free-loss surfaces resembling the chamber cryo-pumps. A single 3D object is used to represent the thruster and is located inside the domain, with a frontal surface that contains the HET annular exit plane (from which plasma and neutrals are injected into the domain), the cathode emission surface, the frontal dielectric surface and the lateral and back metallic surfaces. The mesh resolution is higher near the object, specifically close to the injection plane (1 cm) and decreases near the chamber boundaries. The mesh has 121 nodes along x and y, and 101 nodes along z. Fig. 5 shows the employed mesh, as well as the thruster assembly and the pump surfaces locations.

3.2 Boundary conditions

In this study, different boundary conditions are applied at the material boundaries, for both the PIC and the electron fluid models.

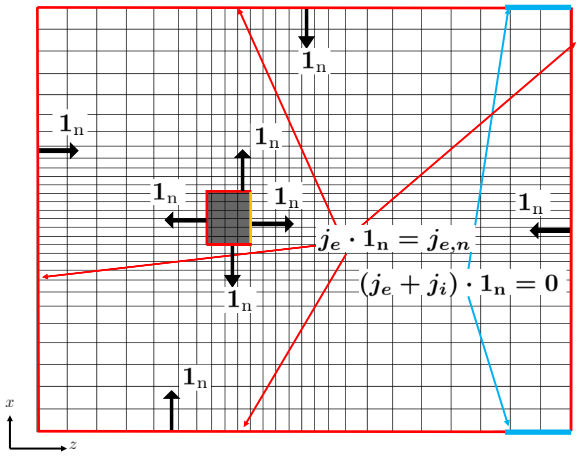

Figure 6: *Boundary conditions at external boundary and thruster object location inside the chamber. Front surface is marked in orange and its BC are defined component-wise (see Fig.7)*

3.2.1 PIC model

Referring to Fig.7, ions and neutrals are injected from the annular channel exit section with known profiles of temperature, density and vector velocity, obtained from the 2D code simulations. Additional neutrals are also injected from the neutralizer surface as shown in Fig.7. When ions and neutrals cross a non-material external boundary, shown by blue solid lines in Fig.6, they are simply removed from the simulation. This type of free loss surface allows to model accurately the behavior of cryo-pumps. If ions hit the front material walls of the thruster or of the chamber, they are recombined into neutrals, which are diffusely re-injected into the simulation domain with a given thermal accommodation coefficient [1]. Neutrals hitting the thruster and chamber walls are also diffusely reflected with the same thermal accommodation. Finally, ions and neutrals re-entering the HET annular channel from the outside are re-injected as neutrals to preserve the total net mass outflow.

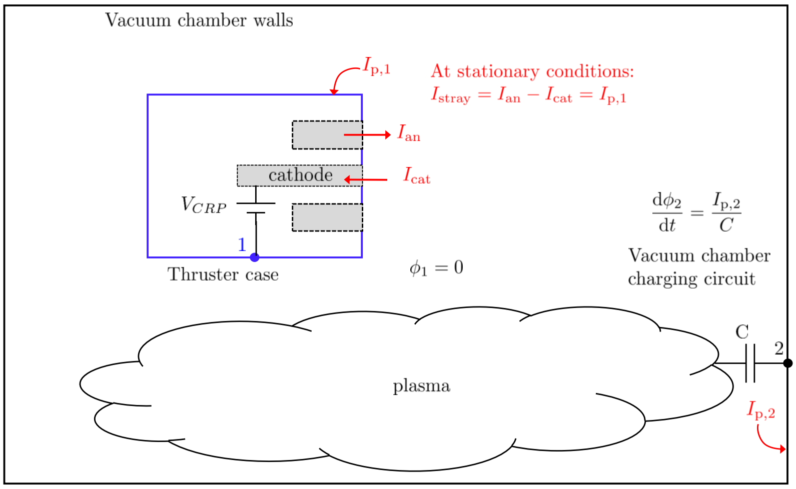

Figure 4: *Equivalent electric circuit schematics.*

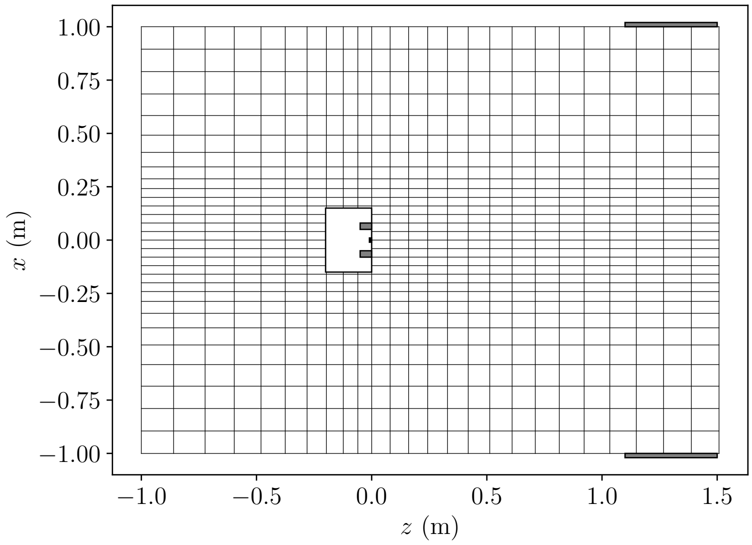

Figure 5: *Employed mesh and main objects in the simulation domain, at $y = 0$. Pump surfaces are located downstream. The black thin lines represent fixed computational coordinates, and, for the sake of clarity, only one every 5 along z and x is shown.*

3.2.2 Electron fluid model

Referring to Fig. 6 and Fig. 7, we have assumed a zero normal electric current condition at all the free-loss boundaries of the simulation domain and also at the front walls of the thruster (therefore assumed to be dielectric) other than the channel and cathode surfaces. On the other hand, prescribed normal electron current densities have been imposed at the exit section of the annular channel, with a free normal electron current at the cathode emission surface (where $\Phi = 0$ and its gradient is thus left free). If $\mathbf{1}_\mathrm{n}$ represents the inward-pointing normal direction to the boundary, as shown in Fig. 1, we prescribe $j_{\mathrm{n,e}} = \boldsymbol{j}_\mathrm{e} \cdot \mathbf{1}_\mathrm{n}$. On the thruster and chamber metallic walls instead, normal electron current densities to be imposed are obtained from a simplified sheath model [1].

3.3 Pump capacity characterization

As typical reference conditions for a vacuum chamber environment, the Sitael's IV4 facility is considered [3]. The chamber (2 meters in diameter and 2.5 m in length) features 6 cold heads as cryo-pumps placed downstream, and reaches typical pressure values of $2 - 3 \cdot 10^{-5}$ mbar during operations, that corresponds to around $6 \cdot 10^{17}$ m^{-3} of background neutrals density.

The numerical domain features a length of 2.5 m and a side of 2 m for the square base of the prism adopted as simulation domain. The non axisymmetry of the domain is expected to have some boundary effects on the symmetry of the solution, but not on its qualitative shape and main investigated effects.

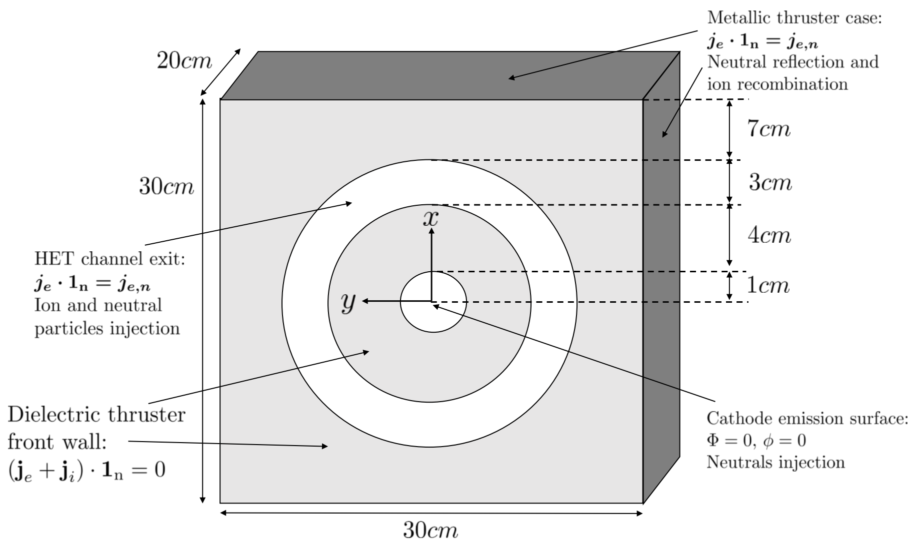

Figure 7: *Boundary conditions and physical dimensions (not in scale) of thuster case and front surface components.*

In order to simulate the plume expansion under the actual experimental conditions, a preliminary study was conducted in order to assess the equivalent pump surfaces needed to reach the experimental background pressure of the chamber. Pumps were placed on the lateral walls of the chamber, downstream and on all the 4 walls of the domain, to be consistent with the experimental geometry and location.

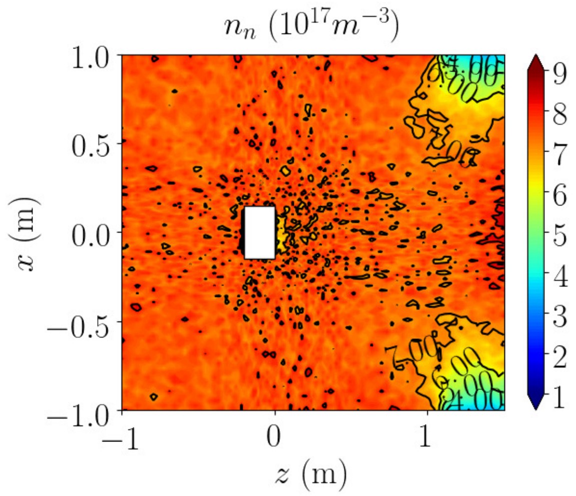

Figure 8: *Neutral background density in the chamber at* $y = 0$

To perform this study, only neutral particles were injected from the thruster assembly, with the total mass flow rate of the thruster and cathode summed together. The steady state background neutrals, resulting from the diffusive reflections on the chamber walls, were then imported as initial background neutrals population for the nominal plasma simulations. This allows to start plasma simulations from a neutral particles quasi-steady state, so the plasma simulation duration can be significantly reduced.

Figure 8 shows the neutral density distribution at steady-state, which is near homogeneous inside the chamber, except near the pumps, where it decreases due to particle loss. The final, steady-state distribution of neutrals, resulting from the diffusive reflections on the material walls at room temperature (300K), were then imported as initial background species in the nominal plasma simulations. This allows to start plasma simulations from a neutral-particle steady state, so the numerical setup is not constrained by the slow neutrals' need to fill up the chamber. The average pressure reached in the chamber (excluding the regions of the pumps and ahead of the thruster) is about $2.6 \cdot 10^{-5} mbar$, while the background density reaches a mean value of $7 \cdot 10^{17} m^{-3}$. These results agree with previous experimental measurements and simulation results for Sitael's IV4 facility [4].

In order to achieve this starting background condition for plasma simulations, a sensitivity analysis was performed, varying the surface area of the 4 downstream free-loss pumps (see Fig.9). As expected, the steady state background pressure decreases as the pump area increases, for a fixed total injected mass flow.

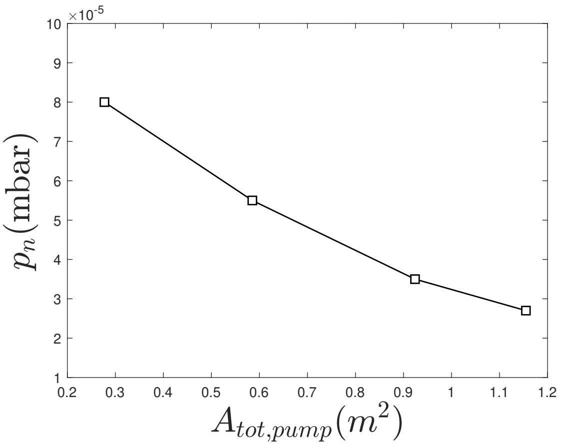

Figure 9: *Sensitivity of the steady state background average pressure in the chamber, when changing the total free-loss downstream pump surface area.*

3.4 Plasma plume expansion in the vacuum chamber

Here the results obtained from the nominal plasma simulations are shown and discussed.
Fig. 10 shows the Hall parameter inside the chamber domain. This is artificially limited by the 2.5% anomalous collisionality assumed in the near plume, while, in the far plume where the magnetic induction field nearly vanishes, the neutrals background further limits it to lower and lower values.

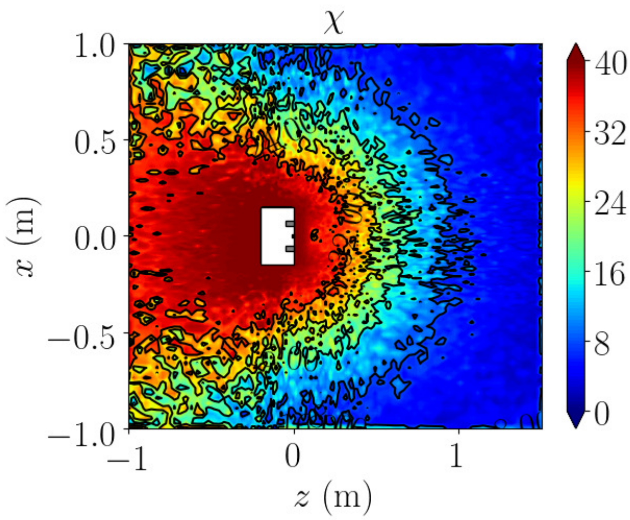

Figure 10: *Effective Hall parameter* χ *at* $y = 0$

Fig.11 shows some relevant plume properties such as electron density, electron temperature and electric potential. The number density of neutrals produced in CEX collisions, and the ionization rate are also shown as representative of the collisional processes taking place in the plume, which are not negligible and constitute an important effect of the high background pressure of the facility. Finally electron, electric and ion current densities are shown, where the effects of the complex magnetic topology are noticeable. The same plume properties are shown in the full chamber domain in Fig. 12. Most of the plasma does not reach the back part of the chamber, which is indeed not quasineutral. Having a look at the electric current, it can be noticed that the metallic chamber, covering most of the external boundary, acts as a global current free condition at steady state, since by definition of floating object, the chamber is not collecting any net current.

It is worth mentioning that the polytropic closure, as well as the low mesh resolution in the near plume region, produce some unrealistic effects on the results, the most important of them being the fact that the cathode plasma is almost equipotential with the plasma at the channel exit.

Finally, Fig.13 some relevant variables associated to the plasma-object interaction, such as the wall impact energies of the relevant species and the time evolution of electric current collected by the objects and of the potential of the latter with respect to the channel exit. The impact energies are shown along an auxiliary coordinate ξ, defined along the whole chamber walls extension at $y = 0$.
The current collected by the chamber is the one needed in the transient phase to reach a floating potential, indeed then the current becomes zero at steady state. Instead the current collected by the thruster case metallic walls (kept at a fixed potential in time) at steady state is not zero and coincides with the stray current.

3.5 Direct Drive "grounded CRP" approach simulation for stray current estimation

The assumed approach for the computation of the stray current evolution is equivalent to the "grounded CRP" one [2], employing a V_{CRP} set between the thruster case wall and the cathode. Since the polytropic model leads to an average of only 15V potential fall between channel exit and cathode, the V_{CRP} values shown in the x-axis at which the stray current becomes negative are expected to be higher than in experiments. The resulting behavior is very similar to that of a probe (see Fig.14), showing an exponential electric current behaviour. In fact, while the ion current is only dimly affected by the metallic case potential (plateau region on the right of the curve), the electron current is the dominating current for positive thruster case potentials (left of the curve).
The dim sensitivity to CRP of the ion current is due to several reasons: (i) the ion density is lower near the lateral and back thruster assembly walls, (ii)

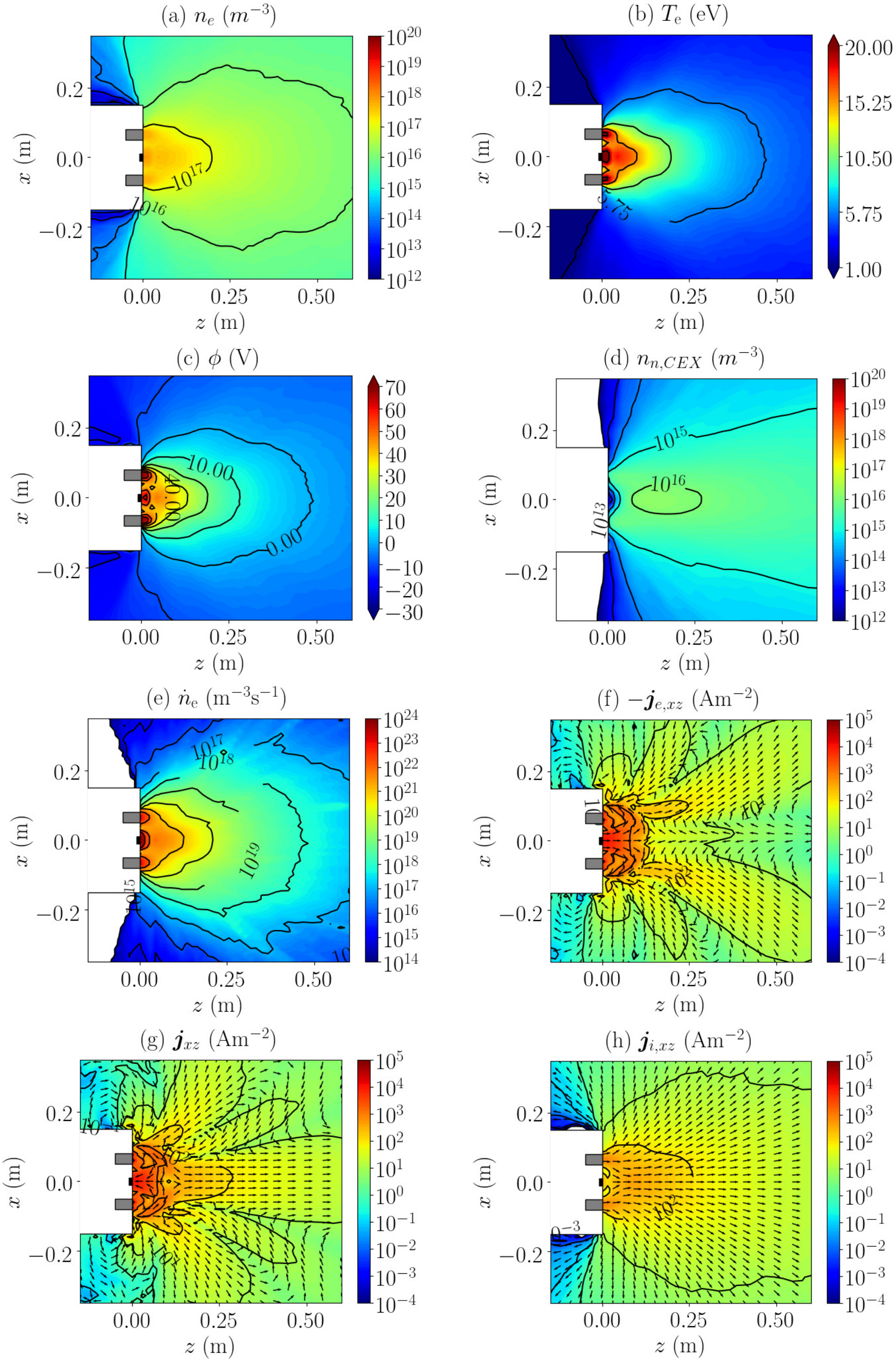

Figure 11: *Nominal simulation results at $y = 0$, zoomed in the near plume, showing: (a) electron density, n_e, (b) electron temperature, T_e, (c) electric potential ϕ, (d) neutral density of Xe atoms from CEX, $n_\mathrm{n,CEX}$, (e) ionization rate, $\dot{n}_\mathrm{e}$, (f) in-plane electron current density magnitude, $j_\mathrm{e,xz}$, (g) in-plane electric current density magnitude, j_xz, (h) in-plane ion current density magnitude, $j_\mathrm{i,xz}$.*

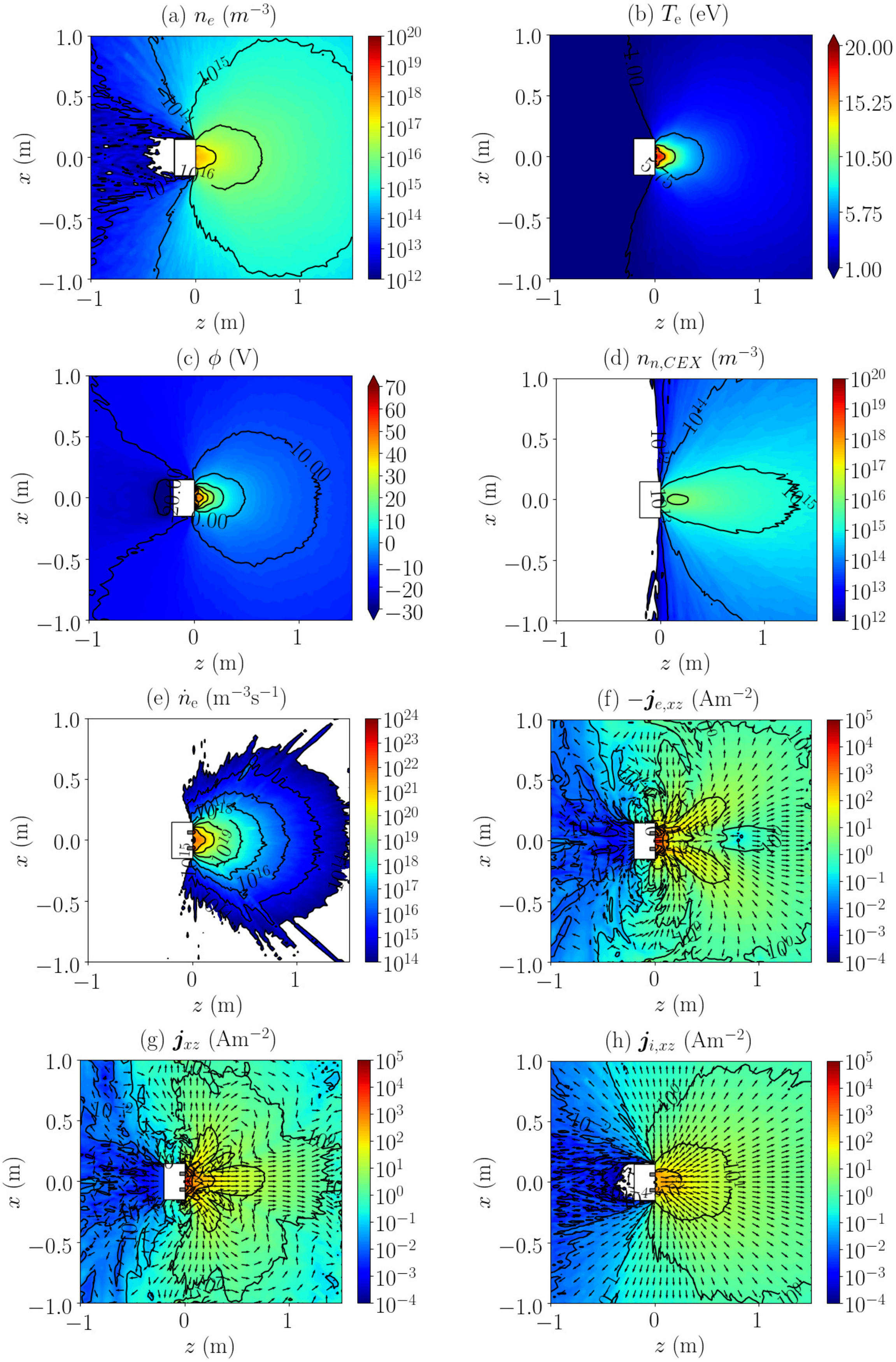

Figure 12: *Nominal simulation results for the whole chamber domain at $y = 0$, showing: (a) electron density, n_e, (b) electron temperature, T_e, (c) electric potential ϕ, (d) neutral density of Xe atoms from CEX, $n_{n,CEX}$, (e) ionization rate, $\dot{n}_e$, (f) in-plane electron current density magnitude , $j_{e,xz}$, (g) in-plane electric current density magnitude, j_{xz}, (h) in-plane ion current density magnitude, $j_{i,xz}$.*

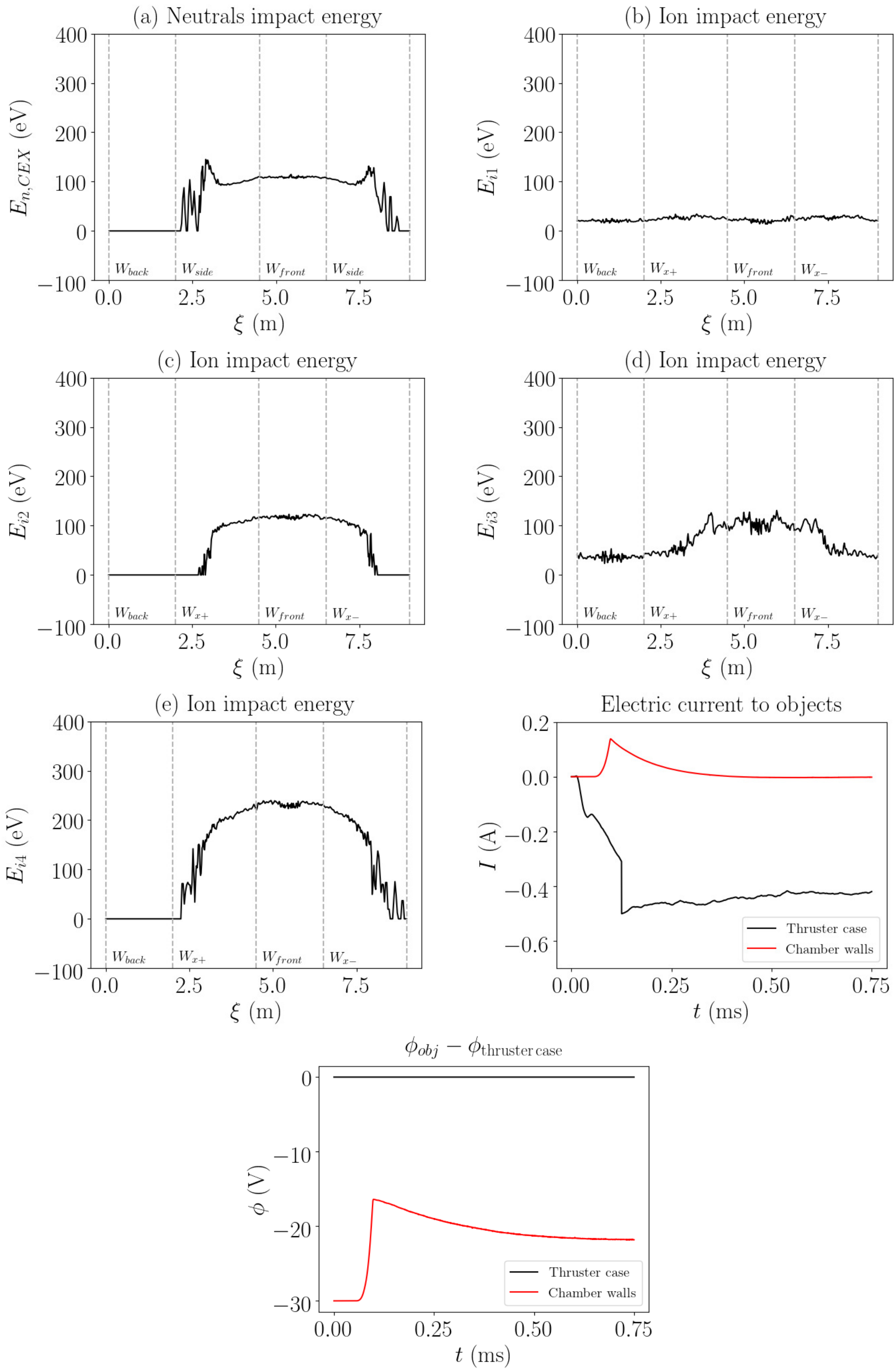

Figure 13: *Relevant variables for plasma-chamber interaction: (a) impact energy of CEX neutrals, (b) impact energy of singly charged ions coming from collision processes, (c) impact energy of singly charged ions injected from the channel exit, (d) impact energy of doubly charged ions coming from collision processes, (e) impact energy of doubly charged ions injected from the channel exit.*

the ion backstream current, generally low, is due to CEX and ionization of the background species in the chamber, (iii) the front face of the thruster is dielectric and collects no net current, (iv) there is no backplate to mimic a S/C behind the thruster that would collect a much larger ion current (the ion stray current depends also on the collecting surface area).

On the other hand, electrons are mainly repulsed by the thruster case when it is very negative relative to the local plasma. When the potential difference between plasma and thruster case becomes comparable to the local electron temperature, a non-negligible fraction of the electron thermal flux reaches the walls: on the left side of Fig.14, in fact, the electron current grows exponentially as the thruster case potential is increased (or the CRP potential decreased).

This first analysis has provided more insight onto the stray current behavior in the direct drive architecture, and has confirmed: (i) the capability of EP2PLUS to simulate positive and negative stray currents in a wide range of V_{CRP} values (even with an equivalent approach adopted to compensate the impossibility to couple the anode/discharge properties with the plume and facility objects), and (ii) the existence of an optimal point in which the stray current collected by the thruster case or S/C is nearly zero.

Further analyses could employ different assembly and material configurations to match the actual values of the stray current obtained in experiments, even if the experimental trend [2] is already quite well represented and explained.

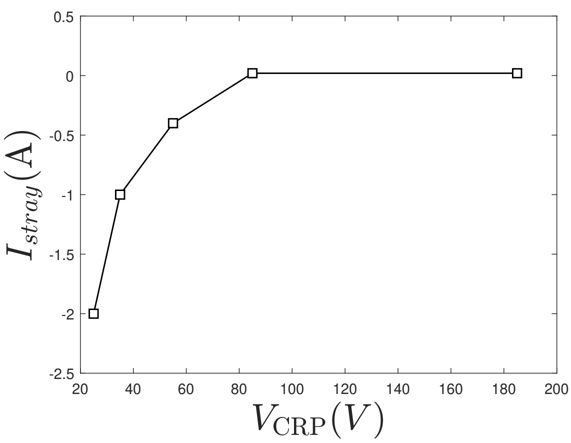

Figure 14: *Stray current to the thruster case metallic walls, vs V_{CRP}. Thruster case metallic walls are taken as reference point for the potential. For high positive V_{CRP}, stray current is basically constant and due to only ions, depending on the objects configuration (collecting more or less backstream current), indeed values here are around 0.02A.*

4 CONCLUSIONS AND FUTURE WORK

The objective of this work was to demonstrate a self-consistent use of a tool for simulations of a HET plume expanding in a ground facility. The synergy and consistency of all the models, even under major simplifying hypotheses - as the polytropic one - still allowed to gain an insight on the behavior of the system, both from the plasma transport point of view and regarding the interaction with objects (including the chamber itself). The code proved to be a helpful tool to understand better the physics and processes involved, being the latter coupled in non trivial ways, which are difficult to understand simply through experimental measurements. The performed simulations show also the effect of the employed magnetic topology on the electric currents that appear within the vacuum chamber.

Future improvements of the models, such as the energy balance equation with heat flux closure for the electron fluid, will make the simulations much more reliable from a physical point of view. Among other improvements, the limitation of the Hall parameter in the near plume through an artificial anomalous collisionality should be overcome, and a mesh optimization for the cylindrical vacuum chamber is also foreseen. Future analysis finally includes studies about the effect of the background pressure (to be compared with experiments [18]) and chamber dimensions, and the simulation of the plume expansion in a free-space scenario to complement the experimental data and suggest behavior trends between chamber and free-space operations.

ACKNOWLEDGMENTS

All the numerical developments of this research have been supported by the project PROMETEO-CM, funded by the Comunidad de Madrid (grant agreement Y2018/NMT-4750). The application to HT20k has been funded by H2020-EU, under the project ASPIRE (grant agreement ID: 101004366).

REFERENCES

[1] Cichocki, F., Domínguez-Vázquez, A., Merino, M., and Ahedo, E., “Hybrid 3D model for the interaction of plasma thruster plumes with

nearby objects," *Plasma Sources Science and Technology*, Vol. 26, No. 12, 2017, pp. 125008.

[2] Ghislanzoni, L., Benetti, L., Tommaso, M., Cesaretti, G., and L., F., "Hall effect thruster direct drive PPU's, experimental investigation of the cathode potential grounding problem," *E3S Web of Conferences 16 (2017) 15002.*.

[3] Misuri, T., Ducci, C., Gregucci, S., Pedrini, D., Cannelli, F., Cesari, U., Nania, F., Vicini, A., Pace, G., Magistro, F., et al., "SITAEL HT100 Thruster Unit, Full Ground Qualification," *Proceedings of the 36th International Electric Propulsion Conference University of Vienna, Vienna, Austria*, 2019, pp. 15–20.

[4] Passaro, A., Vicini, A., and Biagioni, L., "Plasma Thruster Plume Simulation: Effect of Vacuum Chamber Environment," *35th AIAA Plasmadynamics and Lasers Conference*, 2004, p. 2357.

[5] Martínez-Sánchez, M., Navarro-Cavallé, J., and Ahedo, E., "Electron cooling and finite potential drop in a magnetized plasma expansion," *Physics of Plasmas*, Vol. 22, No. 5, 2015, pp. 053501.

[6] Kojima, T., Morita, T., and Yamamoto, N., "Analysis of plasma detachment in the magnetic thrust chamber using full particle-in-cell simulation," *High Energy Density Physics*, Vol. 36, 2020, pp. 100814.

[7] Bird, G., *Molecular Gas Dynamics and the Direct Simulation of Gas Flows*, The Oxford Engineering Science Series, Oxford University Press, Oxford, UK, 1994.

[8] Cichocki, F., Merino, M., and Ahedo, E., "Spacecraft-plasma-debris interaction in an ion beam shepherd mission," *Acta Astronautica*, Vol. 146, 2018, pp. 216–227.

[9] Cichocki, F., Merino, M., and Ahedo, E., "Three-dimensional geomagnetic field effects on a plasma thruster plume expansion," *Acta Astronautica*, Vol. 175, 2020, pp. 190 – 203.

[10] Cichocki, F., Domínguez-Vázquez, A., Merino, M., Fajardo, P., and Ahedo, E., "Three-dimensional neutralizer effects on a Hall-effect thruster near plume," *Acta Astronautica*, Vol. 187, 2021, pp. 498–510.

[11] Perales-Díaz, J., Cichocki, F., Merino, M., and Ahedo, E., "Formation and neutralization of electric charge and current of an ion thruster plume," *Plasma Sources Science and Technology*, Vol. 30, No. 10, 2021, pp. 105023.

[12] Cichocki, F., Domínguez, A., Merino, M., and Ahedo, E., "A 3D hybrid code to study electric thruster plumes," *Space Propulsion Conference 2016*, No. paper 2016-3124968, Association Aéronautique et Astronautique de France, Rome, Italy, May 2-6, 2016.

[13] LeVeque, R. J. et al., *Finite volume methods for hyperbolic problems*, Vol. 31, Cambridge university press, 2002.

[14] Taccogna, F. and Garrigues, L., "Latest progress in Hall thrusters plasma modelling," *Reviews of Modern Plasma Physics*, Vol. 3, No. 1, 2019, pp. 12.

[15] Merino, M., Cichocki, F., and Ahedo, E., "A collisionless Plasma thruster plume expansion model," *Plasma Sources Science and Technology*, Vol. 24, No. 3, 2015, pp. 035006.

[16] Cichocki, F., Navarro-Cavallé, J., Modesti, A., and Ramírez Vázquez, G., "Magnetic Nozzle and RPA Simulations vs. Experiments for a Helicon Plasma Thruster Plume," *Frontiers in Physics*, Vol. 10, 2022.

[17] Domínguez-Vázquez, A., Zhou, J., Fajardo, P., and Ahedo, E., "Analysis of the plasma discharge in a Hall thruster via a hybrid 2D code," 36^{th} *International Electric Propulsion Conference*, No. IEPC-2019-579, Electric Rocket Propulsion Society, Vienna, Austria, 2019.

[18] Piragino, A., Faraji, F., Reza, M., Ferrato, E., Piraino, A., and Andreussi, T., "Background Pressure Effects on the Performance of a 20 kW Magnetically Shielded Hall Thruster Operating in Various Configurations," *Aerospace*, Vol. 8, No. 3, 2021, pp. 69.